 SDHM, vol.3, no.3, pp.121-132, 2007

An Investigation into Active Strain Transfer Analysis in a Piezoceramic Sensor System for Structural Health Monitoring Using the Dual Boundary Element Method

S.P.L. Leme[1], M.H. Aliabadi[2], L.M. Bezerra[1], P.W. Partridge[1]

Abstract: The coupled electromechanical behaviour of a thin piezoceramic sensor bonded to a stiffened panel subjected to membrane mechanical loadings is examined. The sensor is characterised by an electrostatic line model bonded to a damaged panel modelled by the dual boundary element method. Numerical results obtained demonstrate that the proposed method is capable of modelling changes in the signal output due to presence of cracks. Also presented is a numerical model for detecting fatigue crack growth in a stiffened panel using piezoceramic sensors.

Keyword: MEMS, Crack detection

1 Introduction

To ensure structural integrity and hence maintain safety, in-service health and usage monitoring techniques are employed in many engineering areas Staszewski, et al (2004). The state of damage, i.e. structural health, can be established either directly or indirectly. The direct approach checks for the damage type (e.g. cracks, corrosion or delaminations) by applying an appropriate inspection technique. The established inspection techniques vary from visual inspection by the naked eye to passing the structure through a fully automated inspection gantry. In the indirect approach structural performance or rather structural behaviour is measured and compared with the supposedly known global response characteristics of the undamaged structure.

Monitoring crack initiation and growth in advanced material systems and structures is an important task. It has several applications in structural health monitoring (SHM) of aerospace vehicle, civil structures, and other critical mechanical components. The initiation and the growth of damage or cracks can be identified by measuring the appropriate field, such as strain field, electric field etc, which are affected by the change in the localized material and geometrical properties. For example, a straightforward approach is to measure the strain field with the help of a conventional strain gage that is indicative of stress intensity at the crack tip Ali, et al (2005).

Indirect approaches can be based on (a) measurement of the electrical conductivity across the damage zone, (b) measurement of the interferometric change due to change in the refractive index or chance in the opto-acoustic coupling coefficients at the location of damage, (c) measurement from infrared thermography and (d) measurement of the electrical field by introducing the piezoelectric effect in the material system, which falls in the category known as the electromechanical impedance method.

For conventional engineering materials such as metals or fiber reinforced composites, the use of MEMS capacitive sensors is of particular advantage. The basic mechanism of such a sensor is based on the piezoelectric property of the sensor material that produces a change in voltage due to localized deformation during the damage process. However, due to the very small size of such a MEMS sensor, one may need an array of such sensors in order to identify the stress gradient near the damage zone Ali, et al (2005).

In the work presented here, the Dual Boundary Element Method is applied together with the

[1] Departamento de Engenharia Civil e Ambiental, Universidade de Brasília – UnB

[2] Aeronautics Department, Imperial College, University of London UK

coupled effect of the piezoelectric materials to show an efficient way to predict cracks in critical structures and to monitor the crack growth using the concept of MEMS (micro-electro-mechanical system).

2 Dual Boundary Element Method

The Boundary Element Method (BEM) has emerged as a powerful numerical technique for solving crack problems. Its most attractive feature is the reduction of the dimensionality of the problem. This means that high stress gradients near the crack tip can be modelled more efficiently, in comparison with the FEM, as demonstrated by Aliabadi and Rooke (1991). The Dual Boundary Element Method (DBEM), as presented by Portela et al. (1992) and Mi and Aliabadi (1992), is capable of analysing configurations involving any number of edges and embedded cracks in any given geometry. The DBEM was extended to deal with multiple crack growth analysis of stiffened panel by Salgado and Aliabadi (1996), where both continuously and discretely attached stiffeners were considered.

The Dual Boundary Element Method (DBEM), as presented by Aliabadi (1997) is capable of analysing configurations involving any number of edges and embedded cracks in any given geometry. The need for dividing the problem in different regions, common to many boundary element formulations, is avoided by using the displacement equation when collocating at one crack surface and the dual traction equation when collocating at the other crack surface.

The boundary integral displacement equation, for a source point x' at the boundary Γ of a finite sheet is give by:

$$c_{ij}(x')u_j(x') + \int_\Gamma T_{ij}\left(x',x\right)u_j(x)d\Gamma(x) = \int_\Gamma U_{ij}\left(x',x\right)t_j(x)d\Gamma(x)\ldots \ldots + \iint_\Omega U_{ij}(x',X)b_j(X)d\Omega(X) \quad (1)$$

where $T_{ij}(x',x)$ and $U_{ij}(x',x)$ are the Kelvin traction and displacement fundamental solutions, respectively, $u_j(x)$ and $t_j(x)$ are the displacements and tractions at boundary field points x, $b_j(X)$ are body forces acting at field points X inside the domain Ω and c_{ij} is a coefficient that can be determined by rigid body movement considerations.

The corresponding traction boundary integral equation, presented below, can be obtained by differentiation of equation (1), application of the Hooke's law and multiplication by the outward normal,

$$\frac{1}{2}t_j(x') + n_i(x')\int_\Gamma S_{ijk}\left(x',x\right)u_k(x)d\Gamma(x) = n_i(x')\int_\Gamma D_{ijk}\left(x',x\right)t_k(x)d\Gamma(x)\ldots \ldots + n_i(x')\iint_\Omega D_{ijk}(x',X)b_k(X)d\Omega(X) \quad (2)$$

where $S_{ijk}(x',x)$ and $D_{ijk}(x',x)$ contain derivatives of $T_{ij}(x',x)$ and $U_{ij}(x',x)$, respectively and $n_i(x')$ denotes the *i-th* component of the unit outward normal to the boundary at the source point x'.

3 Sensors Equations

The sensors mounted on the plate can be embedded in the Dual Boundary Element Methodology with the use of the compatibility equations. The plate is considered to be thin, so that the interactions forces exchanged with the sensors can be treated as action-reaction body forces. The plate displacement and traction equations can be derived by considering equations (1) and (2) which assume the presence of body forces. If, instead of being distributed over the whole domain, the body forces are confined to straight lines inside it, the domain integrals in equations (1) and (2) reduce to line integrals over the body forces loci. The displacement and traction equations for a thin plate with N sensors continuously bonded to it can thus be written as:

$$c_{ij}(x')u_j(x') + \int_\Gamma T_{ij}(x',x)u_j(x)d\Gamma(x) = \int_\Gamma U_{ij}(x',x)t_j(x)d\Gamma(x)\ldots \ldots + \frac{1}{h}\sum_{n=1}^{N}\int_{\Gamma_{Sn}} U_{ij}(x',X)b_j^{Sn}(X)d\Gamma_{Sn}(X) \quad (3)$$

and

$$\frac{1}{2}t_j(x') + n_i(x')\int_\Gamma S_{ijk}(x',x)u_k(x)d\Gamma(x) = n_i(x')\int_\Gamma D_{ijk}(x',x)t_k(x)d\Gamma(x)\ldots \ldots + n_i(x')\frac{1}{h}\sum_{n=1}^{N}\int_{\Gamma_{Sn}} D_{ijk}(x',X)b_k^{Sn}(X)d\Gamma_{Sn}(X) \tag{4}$$

where Γ_{Sn} stands for the sensors loci, b_k^{Sn} represents the unknown sensor attachment forces and h is the plate thickness.

In-plane loads will be not be imposed on the sensors, and the distributed load acting throughout the length of each sensor will be used to compute its output signal. The relative displacement $\Delta v_j(y)$ with respect to a rigid body motion of the sensor are given by:

$$\begin{aligned}\Delta v_1(y) &= v_1(y) - v_1(0)\\ &= y\chi(0) + \frac{1}{A_S G_S}\int_0^y (y-\eta)f_1(\eta)d\eta\\ &\quad - \frac{1}{I_S E_S}\int_0^y \frac{1}{6}(y-\eta)^3 f_1(\eta)d\eta\end{aligned} \tag{5}$$

$$\begin{aligned}\Delta v_2(y) &= v_2(y) - v_2(0)\\ &= \frac{1}{A_S E_S}\int_0^y (y-\eta)f_2(\eta)d\eta\end{aligned} \tag{6}$$

where the indices 1 and 2 indicate the transverse and the longitudinal direction respectively, y is an arc length parameter $(0 \le y \le L)$, $v_j(0)$ and $\chi(0)$ are rigid body translation and rotation of the reference point $(y = 0)$, A_S is the sensors cross section area, I_S is the sensors cross sectional second moment of inertia, E_S and G_S are the sensor material Young's modulus and shear modulus respectively.

For the sensors to be in equilibrium, the following equations have to be satisfied:

$$\int_0^L f_2(y)dy = 0 \tag{7}$$

$$\int_0^L f_1(y)dy = 0 \tag{8}$$

$$\int_0^L (L-y)\,f_1(y)dy = 0 \tag{9}$$

4 Attachment Conditions

The displacement compatibility conditions for points along the sensors attachment region are based on the assumption that the displacement u_j of a point X' $(X' \in \Gamma_{Sn})$ at the plate and u_j^{Sn} of a corresponding point at the *n-th* sensor, has to be compatible with the shear deformation of the adhesive layer connecting the sensor to the plate. They are expressed, with respect to a reference point X^0 at the same sensor locus $\left(X^0 \in \Gamma_{Sn}\right)$, by N sets of relations as:

$$\Delta u_j(X') - \Delta u_j^{Sn}(X') = \frac{h_{Ad}}{G_{Ad}}\Delta\tau_j^{Ad}(X') \tag{10}$$

where h_{Ad} is the thickness of the adhesive layer, G_{Ad} is the coefficient of shear deformation of the adhesive material, τ_j^{Ad} is the shear stress at the adhesive, $\Delta u_j(X') = u_j(X') - u_j(X^0)$, $\Delta u_j^{Sn}(X') = u_j^{Sn}(X') - u_j^{Sn}(X^0)$, $\Delta\tau_j^{Ad}(X') = \tau_j^{Ad}(X') - \tau_j^{Ad}(X^0)$. For the line sensors, the adhesive shear stress τ_j^{Ad} are equal in value to the attachment forces b_j^{Sn} divided by the width of the adhesive line w_{Ad}. The displacement compatibility equation can be written in terms of the body forces as:

$$\Delta u_j(X') - \Delta u_j^{Sn}(X') = \Phi_{Ad}\Delta b_j^{Sn}(X') \tag{11}$$

where $\Delta b_j^{Sn}(X') = b_j^{Sn}(X') - b_j^{Sn}(X^0)$ and

$$\Phi_{Ad} = \frac{h_{Ad}}{w_{Ad}G_{Ad}} \tag{12}$$

is the coefficient of shear deformation of the adhesive.

If the reference point X^0 is taken to coincide with the sensor starting point $(y = 0)$, the relative displacement Δu_j^{Sn} in equation (11) can be expressed as a function of the unknown interaction forces b_j^{Sn}, by using the expressions (5) and (6). The relationship between the relative displacements and forces expressed in terms of the plate and the sensors coordinate systems is given by:

$$\Delta u_i^{Sn} = \Theta_{ij}^{Sn}\Delta v_j^{Sn} \tag{13}$$

and

$$b_i^{Sn} = \Theta_{ij}^{Sn} f_j^{Sn} \tag{14}$$

The transformation matrix being:

$$\Theta^{Sn} = \begin{bmatrix} +\cos\varphi^{Sn} & -\sin\varphi^{Sn} \\ +\sin\varphi^{Sn} & +\cos\varphi^{Sn} \end{bmatrix} \tag{15}$$

where ϕ^{Sn} is the angle between the plate direction x_2 and the *n-th* sensor axis.

The plate relative displacements $\Delta u_j(X') = u_j(X') - u_j(X^0)$ in equation (11) can be then finally written as:

$$\begin{aligned} \Delta u_j(X') = & \int_\Gamma \left[U_{ij}(X',x) - U_{ij}(X^0,x)\right] t_j(x) d\Gamma(x) \\ & - \int_\Gamma \left[T_{ij}(X',x) - T_{ij}(X^0,x)\right] u_j(x) d\Gamma(x) \\ & + \dots \\ & + \frac{1}{h} \sum_{n=1}^{N} \int_{\Gamma_{Sn}} \left[U_{ij}(X',X) - U_{ij}(X^0,X)\right] \\ & \cdot b_j^{Sn}(X) d\Gamma_{Sn}(X) \end{aligned} \tag{16}$$

5 Piezoelectric Effect

According to the IEEE compact matrix notation [see IEEE Standards (1978)], the coupled electromechanical constitutive equations of a linear piezoelectric material are written as
direct piezoelectric effect:

$$D = \varepsilon^T E + d\sigma \tag{17}$$

converse piezoelectric effect:

$$\varepsilon = s^E \sigma + d' E \tag{18}$$

where D (charge/area) and E (voltage/length) are the electric displacement and electric fields respectively. ε and σ are the mechanical strain and stress, d, ε^T and s^E are the piezoelectric strain constant, dielectric permittivity and compliance constant, respectively. The superscripts E and T indicate values of the constant obtained at a constant electrical and stress fields, respectively.

For the sensor model, according to Lin and Yuan (2001) and assuming that the sensor is sufficiently small to consider the strain constant inside the sensor area, the output voltage can be written as

$$V_{out} = \frac{d_{31} E_p h_p \varepsilon_R}{4 K_3 \varepsilon_0 \pi (1 - \upsilon_p)} \tag{19}$$

where d_{31} is the piezoelectric charge coefficient equal to 130×10^{-12} m V^{-1}, E_p is the young modulus equal to 76×10^9, h_p is the thickness, K_3 is the relative dielectric constant equal to 1280, and ε_0 is the dielectric permittivity of a free space equal to 8.85×10^{-12} for PKI-402 piezoelectric sensor.

6 Evaluation of the Static Strain to Crack Identification

As demonstrated in Liang and Hwu (2001) accurate on-line measurement of static strains is possible by applying highly developed smart materials. Difference in signals from the pristine state to a damaged state can indicate the position of the crack and also its size.

7 Numerical Examples

In order to allow for comparisons, similar examples as those presented in Tua et al (2004) will be studied. In Tua et al (2004) it was shown that Lamb waves can be used to detect cracks. Here static evaluation of strain fields in a plate will be used as an alternative way of demonstrating the problem of crack detection.

First, we should demonstrate that for the pristine state, the position of sensors in the plate does not alter the value of the output voltage in the sensors. A square plate of width 600mm is considered in figure 1. Also shown in the figure is the distribution of the sensors. A boundary element mesh with 24 quadratics elements was used to analyse the problem.

The table 2 shows the properties from the PZT sensors.

Figure 2 presents the output voltage related to different positions of sensors on the plate. The maximum difference for the output voltage is 0.13 %, and therefore considered as constant and not influenced by the position of sensors in the plate.

8 Determination of a Crack in a Square Aluminium Plate

In all numerical examples analysed the coefficient of shear deformation for the adhesive is taken as

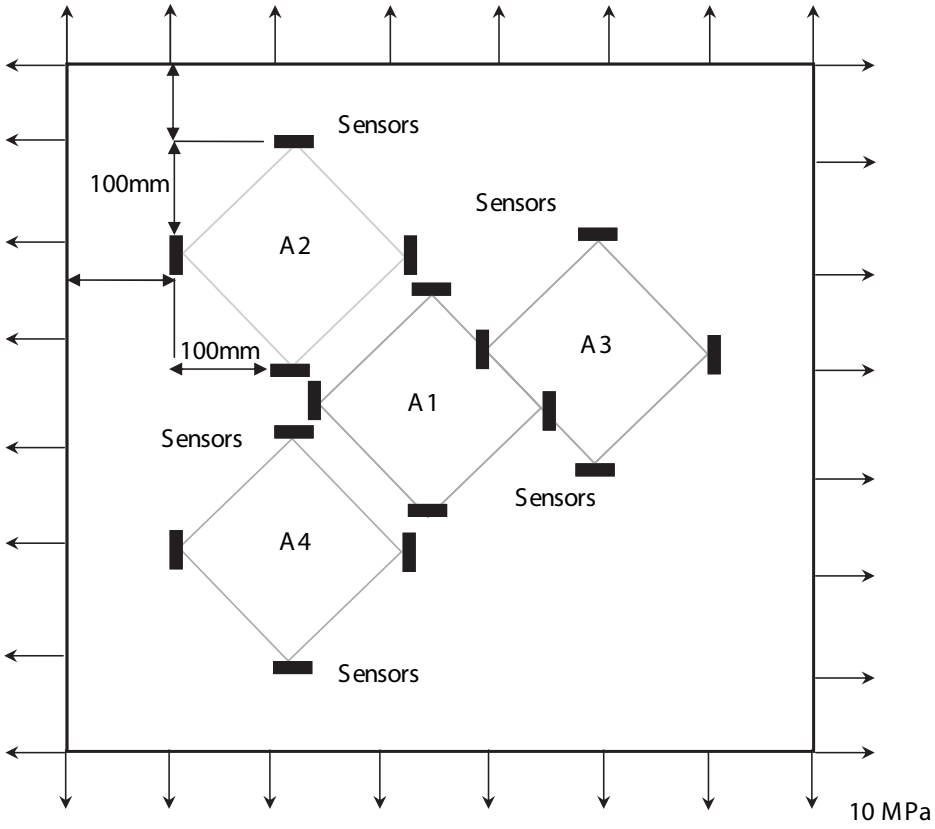

Figure 1: Aluminium plate with different position of 4 sensors.

Table 1: Geometrical and material properties of aluminium plate.

Dimensions (mm^3)	$600\times600\times2$
Young's modulus, E (GPa)	72.5
Shear modulus, G (GPa)	27.25
Mass density, ρ (kg m^{-3})	2700
Poisson Coefficient, υ	0.33

Table 2: Geometrical and material properties of PZT – ceramic (PKI-402)

Dimensions (mm^3)	$8\times8\times0.5$
Young's modulus, E_p (GPa)	76
Shear modulus, G_p (GPa)	29
Mass density, ρ_p (kg m^{-3})	7600
Poisson Coefficient, υ_p	0.31
Relative dielectric constant K_3	1280
Piezoelectric charge coefficient d_{31}, (m $V^{-1)}$	130×10^{-12}
Thickness, h (cm)	0.05
Dielectric permittivity of a free space, ε_0 (F m^{-1})	8.85×10^{-12} F m^{-1}

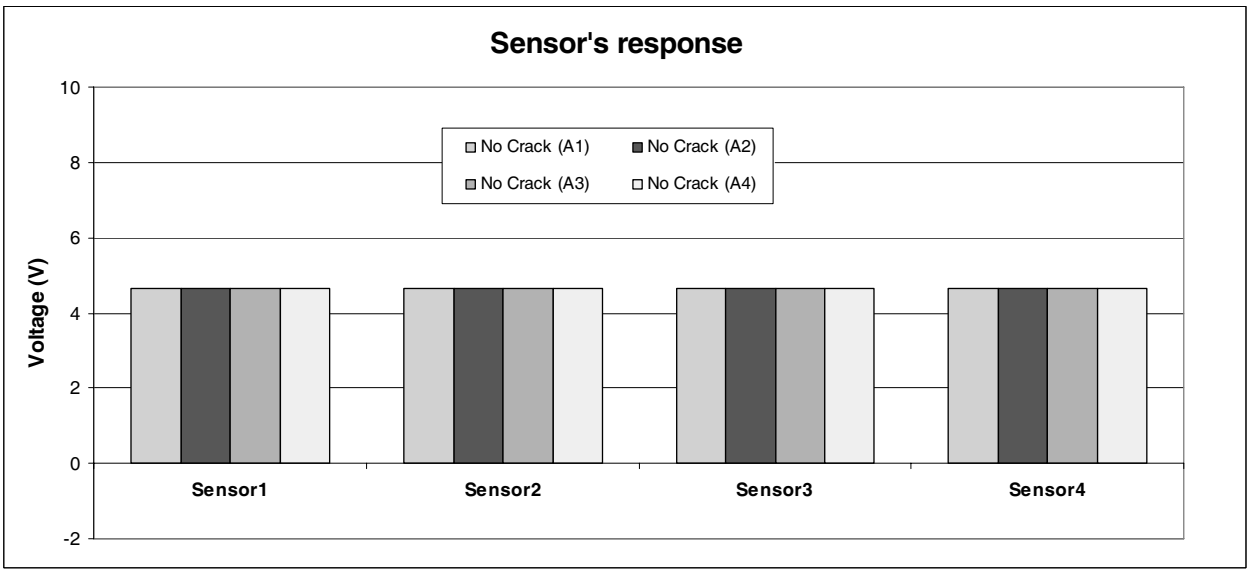

Figure 2: Output from the sensors in different position on the plate.

0.085. Different values to this parameter can be considered if deemed necessary. The mesh utilized consists of 28 quadratic elements.

A crack of 2 mm is introduced into the square plate analysed previously. To investigate the influence of crack on the sensor output, different proximities of a crack to sensors are analysed as shown in figure 3. As it can be observed from figure 4, a change in signal is detected when sensor 1 is within a distance approximately three times the length of the sensor. It can also be seen that a greater signal voltage is achieved when the crack is in direction perpendicular to the sensor. Therefore, both relative proximity and orientation appear to influence the output signal. The results indicate no change to the signal from sensors 2 to 4, which can therefore be considered too far from the crack

Next, the influence of crack size on the sensor signal is investigated. Several cracks of different lengths are introduced under sensor 4 as shown in figure 5. This is purely a theoretical case as in practice the resulting strain due to a crack would be too large for sensor 4 and the sensor will break. In figure 6 the resulting signals are shown. As it can be seen there are considerable increases in the signal as the crack size increases.

9 Example of Multiple-Crack Growth Propagation in Stiffened Panel

The DBEM was successfully applied by Salgado and Aliabadi (1996) to predict multiple crack growth in a stiffened sheet. Here the same example is used there to demonstrate the use of sensors in detecting crack growth.

Consider the panel with riveted stiffeners presented in figure 7. The sheet is 2.3mm thick and the stiffeners are made of aluminium alloy A2024-T3 with the following properties: Young's modulus: 78 500 MPa; Poisson's Coefficient: 0.32; shear modulus: 29 000 MPa. The stiffeners cross-sectional properties are: area: 300 mm^2; second moment of inertia: 1800 mm^4. The rivets are considered to be rigid. In figure 8 the same structure is presented but now with two cracks on the plate, one emanating from a rivet hole in the centre of the panel and the second emanating from the circular opening. The correspondent rivet is rendered ineffective and the central stiffener is broken. The panel is subjected to tensile stress of 10 MPa, applied at the top and bottom edges. The stiffeners are subjected to the same stresses applied at their extreme points.

The difference in the signal captured by the sensors from the pristine state and the crack growth's initial state is shown in figure 9. From the fig-

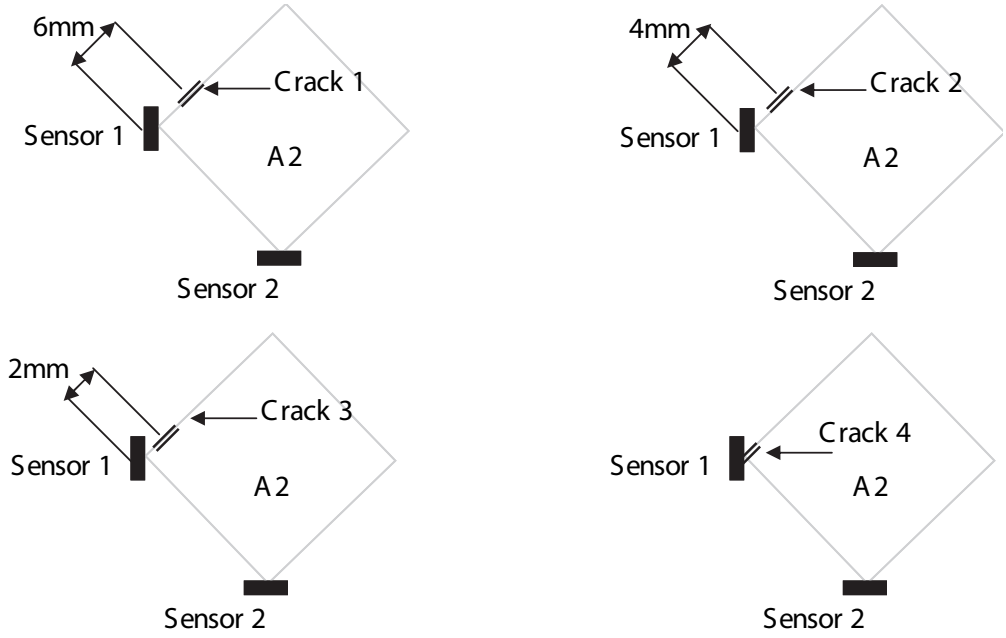

Figure 3: Sensitivity of the signal to the relative position of the sensors and the crack. – (a) Sensor's position to crack 1; (b) Sensor's position to crack 2; (c) Sensor's position to crack 3; (d) Sensor's position to crack 4.

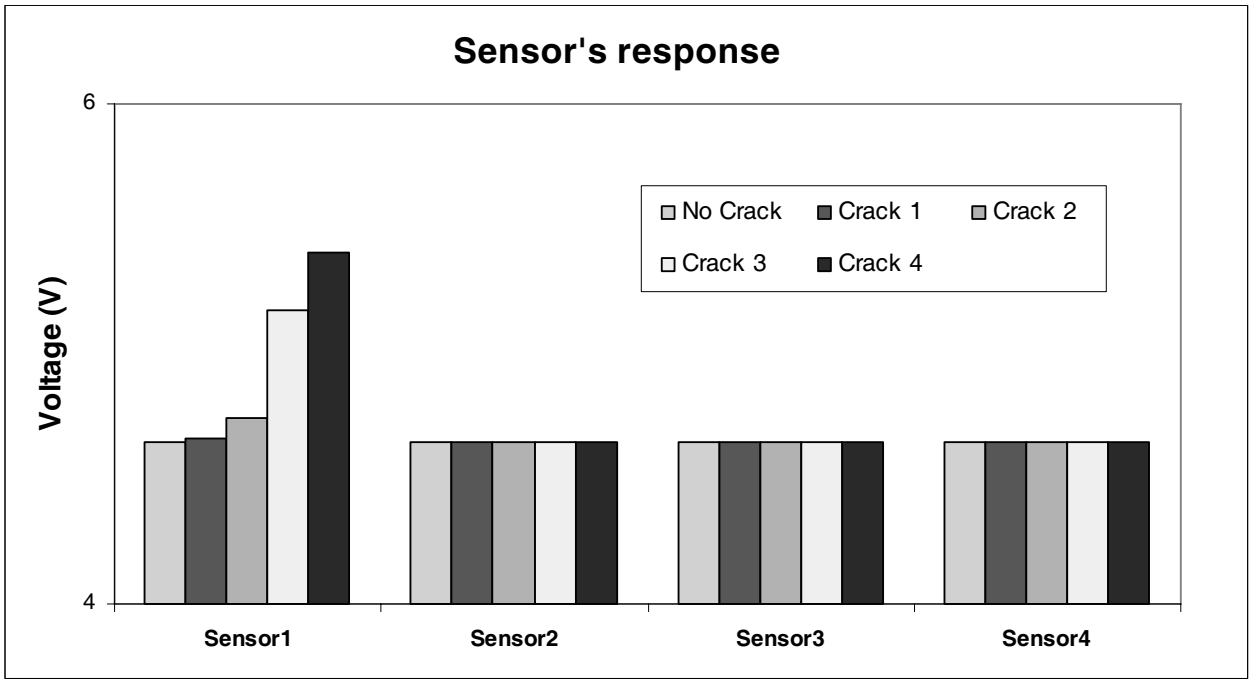

Figure 4: Output from the sensors.

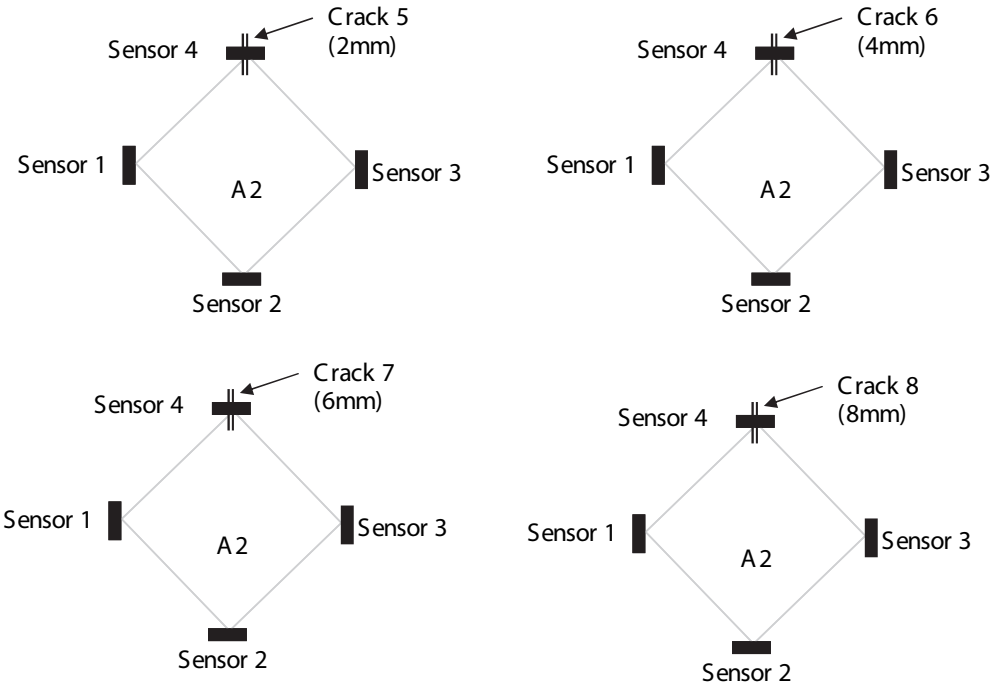

Figure 5: Sensitivity of the signal to different size cracks

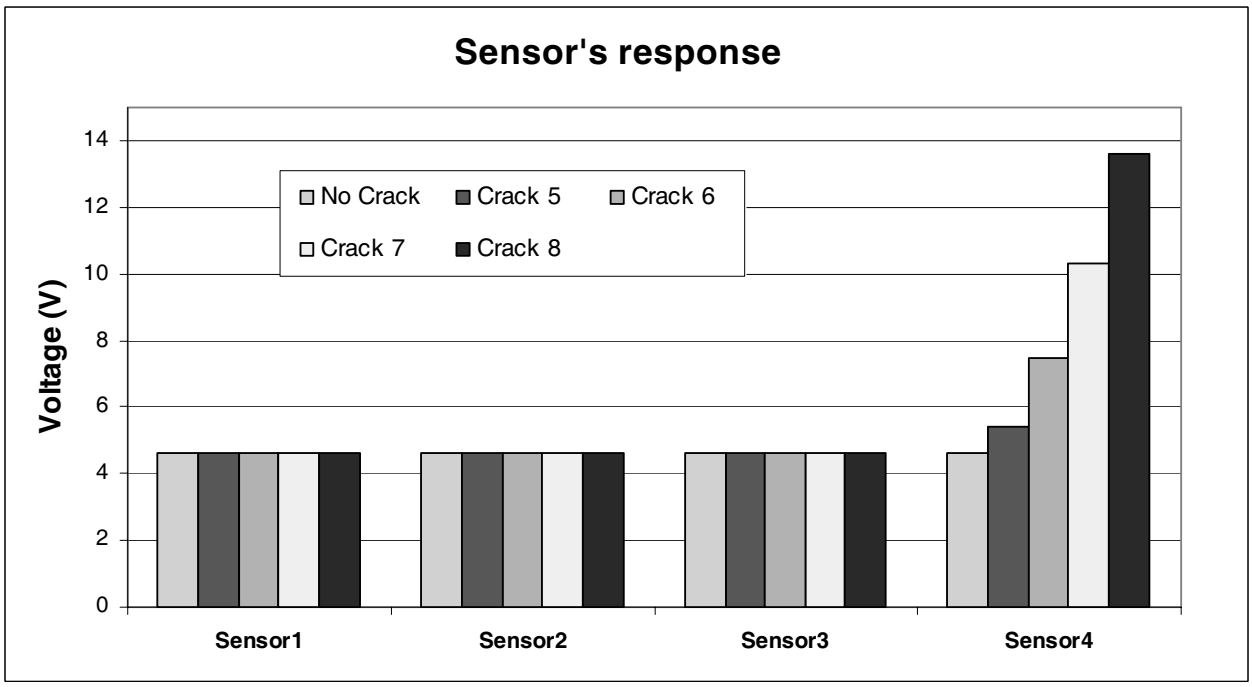

Figure 6: Output from the sensors with increasing crack size.

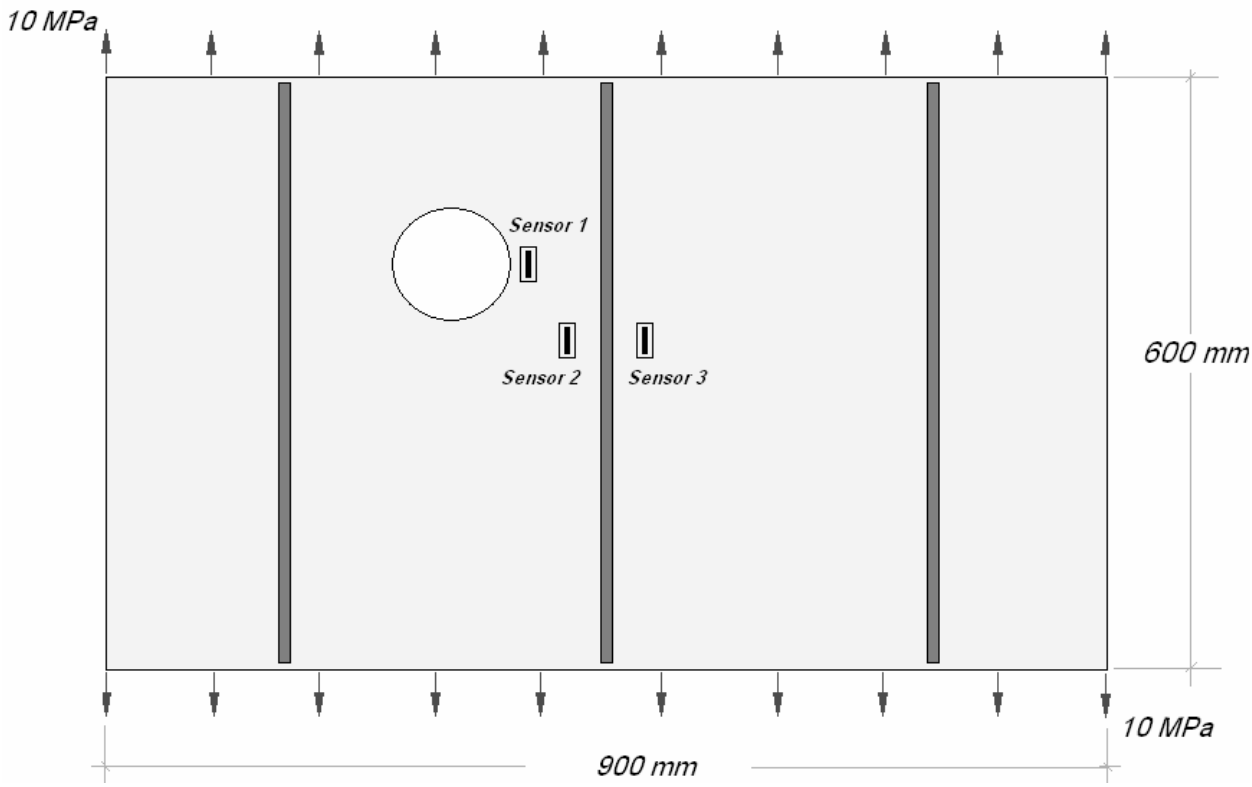

Figure 7: Aluminium panel with rivet stiffeners.

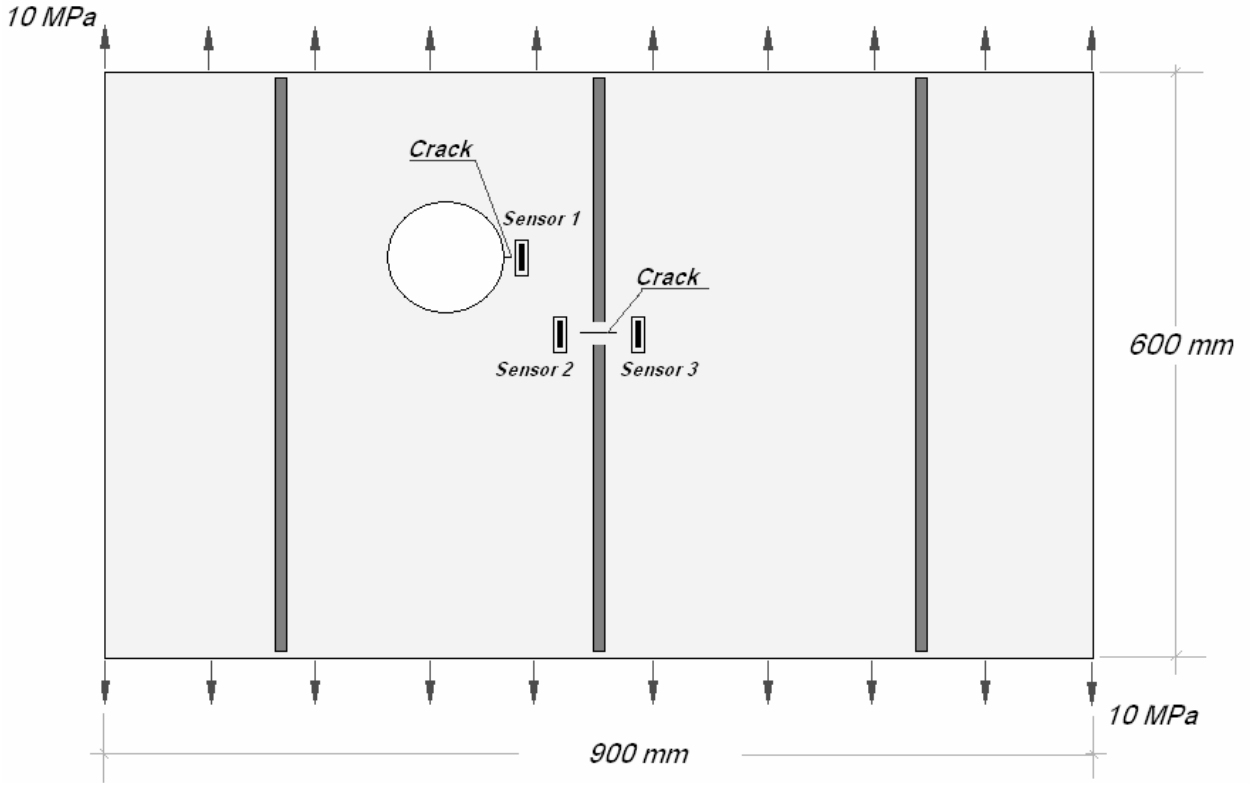

Figure 8: Aluminium panel with rivet stiffeners and cracks.

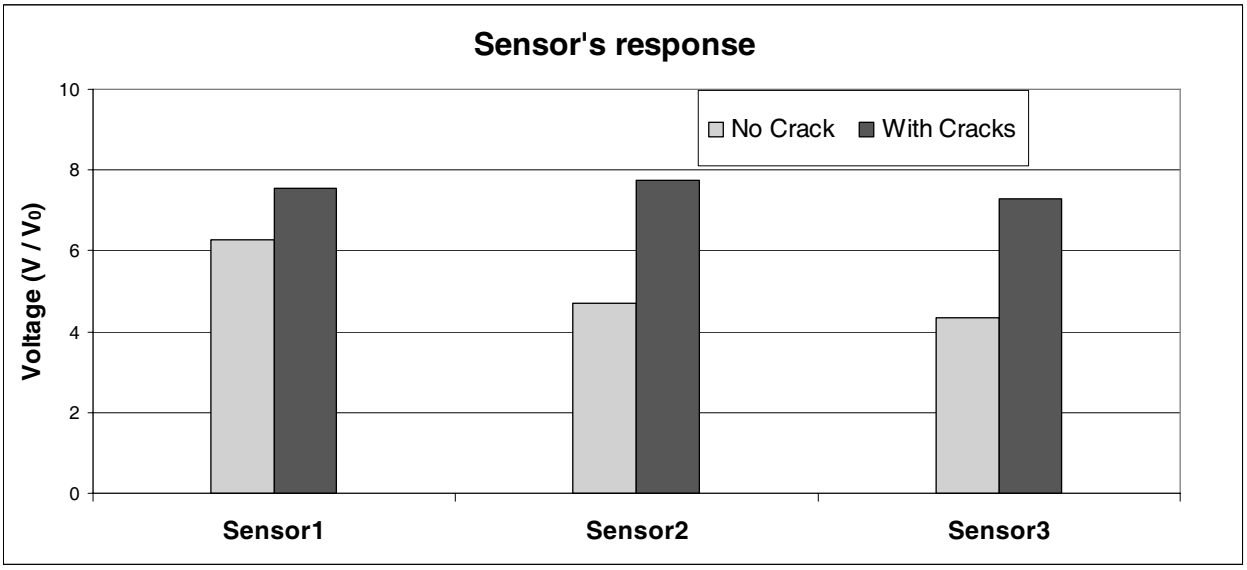

Figure 9: Signal in the sensors for the pristine state and initial state of crack growth.

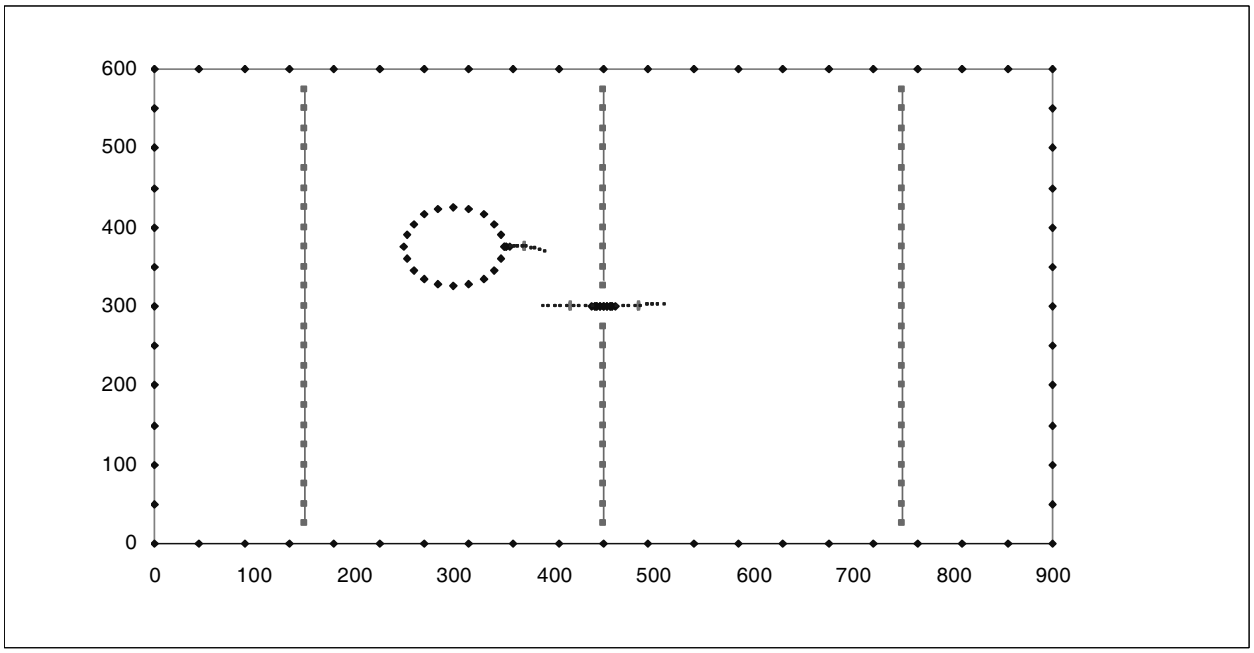

Figure 10: Crack growth path.

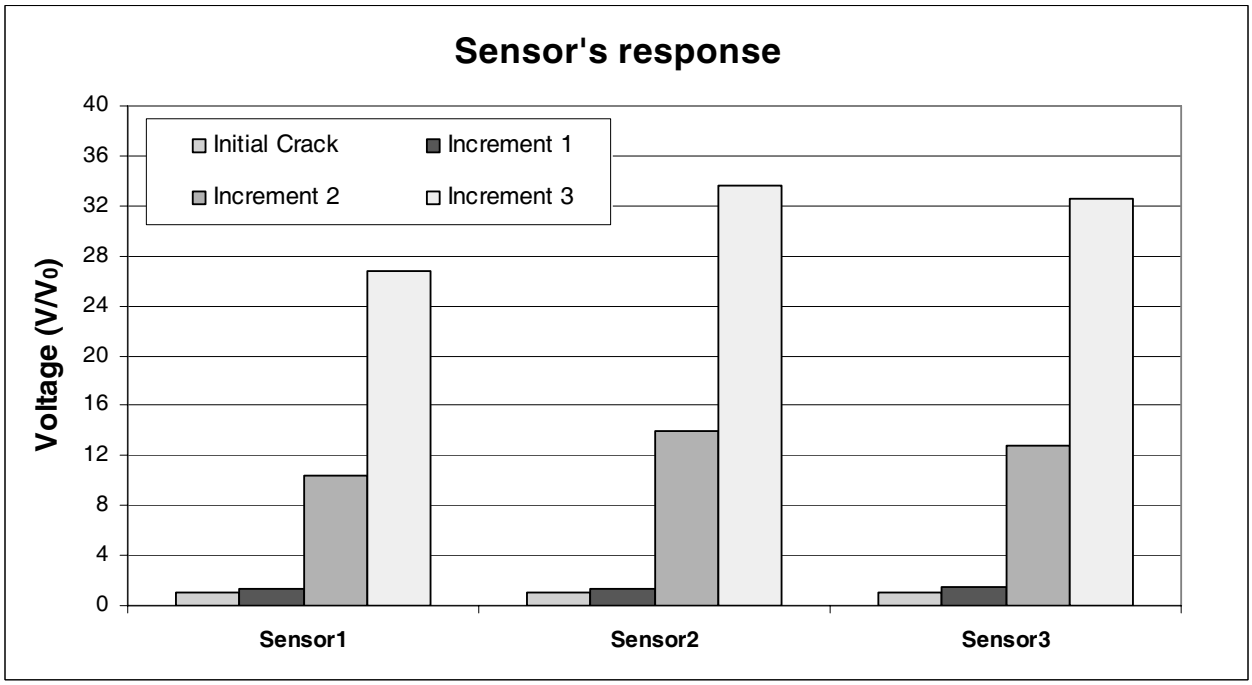

Figure 11: Signal output for different increments of crack extension.

ure we can note a difference between the signal of the sensor 1 with sensors 2 and 3, which is due to the presence of the hole. The introduction of the cracks into the panel results in a greater relaxation of the strain gradients over the panel and hence more uniform signal output from the sensors.

Next, we investigate the use of the sensors in detecting fatigue crack growth. The crack growth parameters used are: Paris law coefficients: $C_p = 0.183 \times 10^{-11}$ and $m_p = 3.284$. Fatigue crack growth is simulated, considering that the load is applied in cycles of constant amplitude, the stress ratio being 0. Four crack extension increments were calculated. The final path to the cracks growth is presented in figure 10.

In the Figure 10 we can see the behaviour of the signal produced by the sensors in comparison with the initial signal. The crack growth can be monitored since the values change significantly with small increments of the crack.

10 Conclusions

Accurate computation of strain fields inside cracked plates and simple modelling of the sensorised panel with the proposed Dual Boundary Element Method allows for possibility of structural health monitoring using static strain fields. It was noted that the calculated strain field can monitor with precision the behaviour of the cracks inside plates.

Acknowledgement: The authors from Universidade de Brasília gratefully acknowledge CNPq (Brazilian National Research Council) and CAPES Foundation (Foundation for the Coordination of Higher Education and Graduate Training) for their support for this research.

References

Staszewski, W.; Boller, C.; Tomlinson, G. (2004): *Health Monitoring of Aerospace Structures – Smart Sensor Technologies and signal processing*, John Wiley & Sons, Ltd. England.

Ali, R.; Mohapatra, D.R.; Gopalakrishnan, S. (2005): Constrained piezoelectric thin film for sensing of subsurface cracks, *Smart Materials and Structures*, 14, 376–386.

Aliabadi, M.H.; Rooke, D.P. (1991): *Numerical Fracture Mechanics Solid Mechanics and its Applications*, Computational Mechanics Publica-

tions.

Portela, A.; Aliabadi, M.H.; Rooke, D.P. (1992): Dual boundary Element Method, effective implementation for crack problems, *International Journal of Numerical Methods in Engineering*, 33, 1269–1287.

Salgado, N.K.; Aliabadi, M.H. (1996): The application of the Dual Boundary Element Method to the analysis of cracked stiffened panels, *Engineering Fracture Mechanics*, 54, 1, 91–105.

Aliabadi, M.H. (1997): A new generation of boundary element methods in fracture mechanics, *International Journal for Fracture*, 86, 91–125.

Liang, Y.C.; Hwu, C. (2001): On-line identification of holes/cracks in composite structures, *Smart Materials and Structures*, 10, 599–609.

IEEE (1978): *Piezoelectricity IEEE Standard 176*, New York.

Lin, X.; Yuan, F.G. (2001): Diagnostic Lamb waves in an integrated piezoelectric sensor/actuator plate: analytical and experimental studies, *Smart Materials and Structures*, 10, 907–913.

Tua, P.S.; Quek, S.T.; Wang, Q. (2004): Detection of cracks in plates using piezo-actuated Lamb waves, *Smart Materials and Structures*, 13, 643–660.